Supporting Information for "The DOE E3SM Model Version 2: Overview of the physical model and initial model evaluation"

Jean-Christophe Golaz[1], Luke P. Van Roekel[2], Xue Zheng[1], Andrew F. Roberts[2], Jonathan D. Wolfe[2], Wuyin Lin[3], Andrew M. Bradley[4], Qi Tang[1], Mathew E. Maltrud[2], Ryan M. Forsyth[1], Chengzhu Zhang[1], Tian Zhou[5], Kai Zhang[5], Charles S. Zender[6], Mingxuan Wu[5], Hailong Wang[5], Adrian K. Turner[2], Balwinder Singh[5], Jadwiga H. Richter[7], Yi Qin[1], Mark R. Petersen[2], Azamat Mametjanov[8], Po-Lun Ma[5], Vincent E. Larson[9,5], Jayesh Krishna[8], Noel D. Keen[10], Nicole Jeffery[2], Elizabeth C. Hunke[2], Walter M. Hannah[1], Oksana Guba[4], Brian M. Griffin[9], Yan Feng[8], Darren Engwirda[2], Alan V. Di Vittorio[10], Cheng Dang[11,12*], LeAnn M. Conlon[2], Chih-Chieh-Jack Chen[7], Michael A. Brunke[13], Gautam Bisht[5], James J. Benedict[2], Xylar S. Asay-Davis[2], Yuying Zhang[1], Meng Zhang[1], Xubin Zeng[13], Shaocheng Xie[1], Phillip J. Wolfram[2], Tom Vo[1], Milena Veneziani[2], Teklu K. Tesfa[5], Sarat Sreepathi[14], Andrew G. Salinger[4], J. E. Jack Reeves Eyre[13,15*], Michael J. Prather[11], Salil Mahajan[14], Qing Li[2,16*], Philip W. Jones[2], Robert L. Jacob[8], Gunther W. Huebler[9], Xianglei Huang[17], Benjamin R. Hillman[4], Bryce E. Harrop[5], James G. Foucar[4], Yilin Fang[5], Darin S. Comeau[2], Peter M. Caldwell[1], Tony Bartoletti[1], Karthik Balaguru[5], Mark A. Taylor[4], Renata B. McCoy[1], L. Ruby Leung[5], David C. Bader[1],

[1]Lawrence Livermore National Laboratory, Livermore, CA, USA

[2]Los Alamos National Laboratory, Los Alamos, NM, USA

[3]Brookhaven National Laboratory, Upton, NY, USA

[4]Sandia National Laboratories, Albuquerque, NM, USA

[5]Pacific Northwest National Laboratory, Richland, WA, USA

[6]Departments of Earth System Science and Computer Science, University of California, Irvine, CA, USA

[7]Climate and Global Dynamics Laboratory, National Center for Atmospheric Research, Boulder, CO, USA

[8]Argonne National Laboratory, Lemont, IL, USA

[9]Department of Mathematical Sciences, University of Wisconsin-Milwaukee, Milwaukee, WI, USA

[10]Lawrence Berkeley National Laboratory, Berkeley, CA, USA

[11]Department of Earth System Science, University of California, Irvine, CA, USA

[12]Joint Center for Satellite Data Assimilation, Boulder, CO, USA

[13]Department of Hydrology and Atmospheric Sciences, University of Arizona, Tucson, AZ, USA

[14]Oak Ridge National Laboratory, Oak Ridge, TN, USA

[15]NOAA NCEP/CPC, College Park, MD, USA

[16]The Hong Kong University of Science and Technology (Guangzhou), Guangzhou, Guangdong, China

[17]Department of Climate and Space Sciences and Engineering, University of Michigan, Ann Arbor, MI, USA

*Current affiliation

Contents of this file

1. Figures S1 to S15.

2. Table S1

Additional Supporting Information (Files uploaded separately)

1. Table S1: Data from Figures 7 and S15 is available in external file '`cmip6.csv`'. Rows correspond to CMIP6 models (first member of historical simulations) or E3SMv2 configurations and column correspond to different fields and seasons. Values are RMSE against relevant observations. Missing values (models for which a specific variable is not available) are indicated by '`--`'. Underlying E3SM Diags comparison figures are available on-line (`https://portal.nersc.gov/project/e3sm/CMIP6_E3SMv2_Golaz_et_al_2022`) . See main text for additional information.

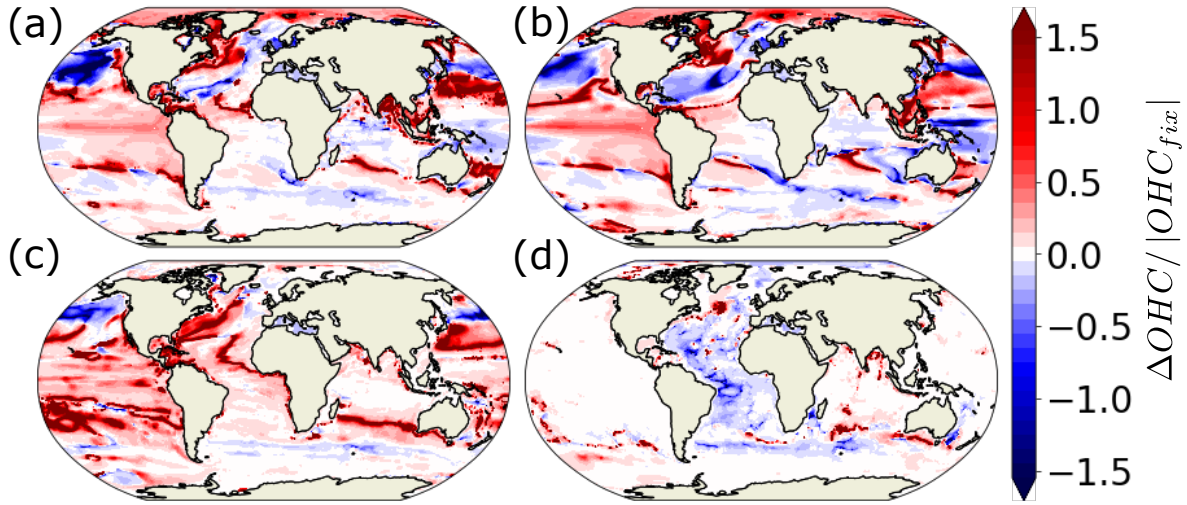

Figure S1. Percent change in ocean heat content anomalies between the simulation with the advection bug and with the bug fixed, i.e., $(OHC_{fix} - OHC_{bug})/\,|OHC_{fix}|$, (a) Full depth, (b) 0-700m, (c) 700-2000m, and (d) 2000m - Bottom.

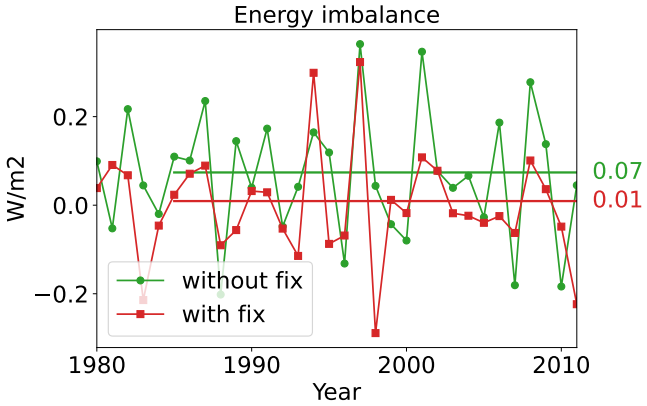

Figure S2. Energy imbalance (diagnosed as the difference between the net fluxes at the top and the surface) for atmosphere simulations with and without energy fix in the gravity wave drag parametrization. Horizontal lines and corresponding values to the right of the plot indicate average values of the imbalance.

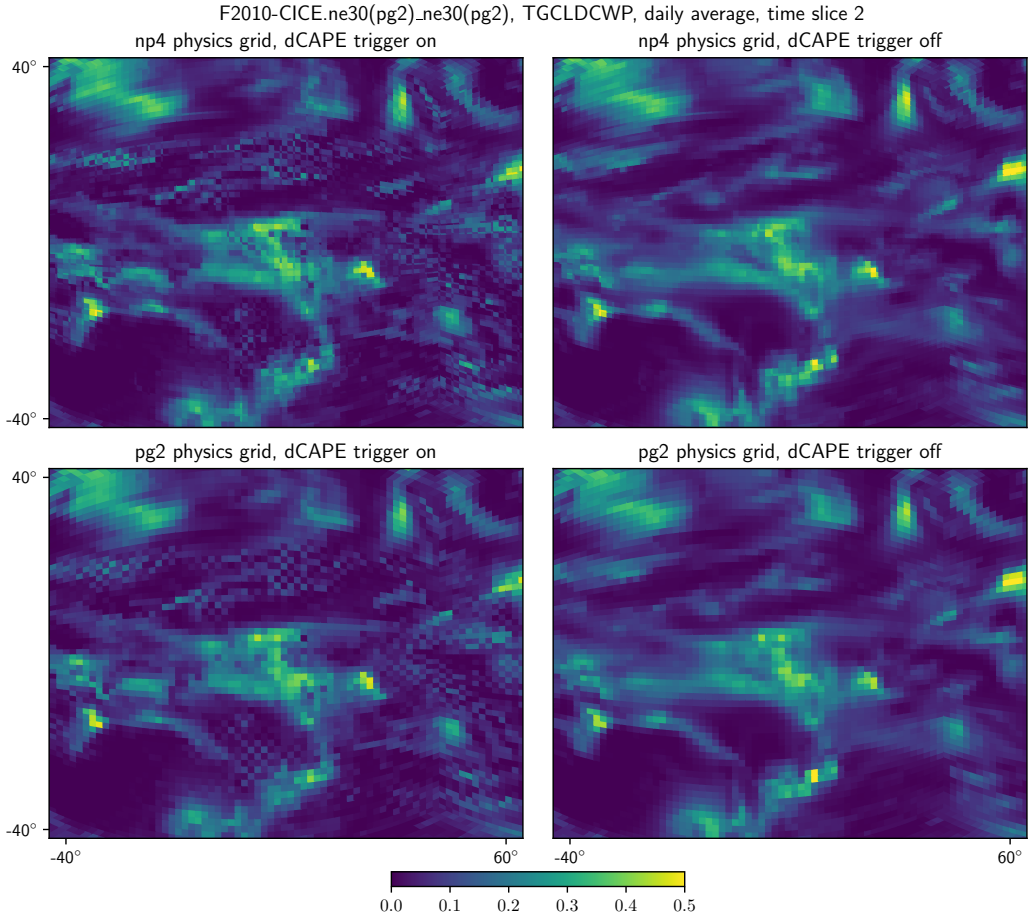

Figure S3. Daily average output of the total grid-box cloud liquid water path (TGCLDLWP) field in the second time slice of four low-resolution atmosphere simulations: physics on the np4 grid, as in E3SMv1 (top row; F2010-CICE.ne30_ne30), physics on the pg2 grid (bottom row; F2010-CICE.ne30pg2_ne30pg2), with the dCAPE trigger on (left column), and with the dCAPE trigger off (right column).

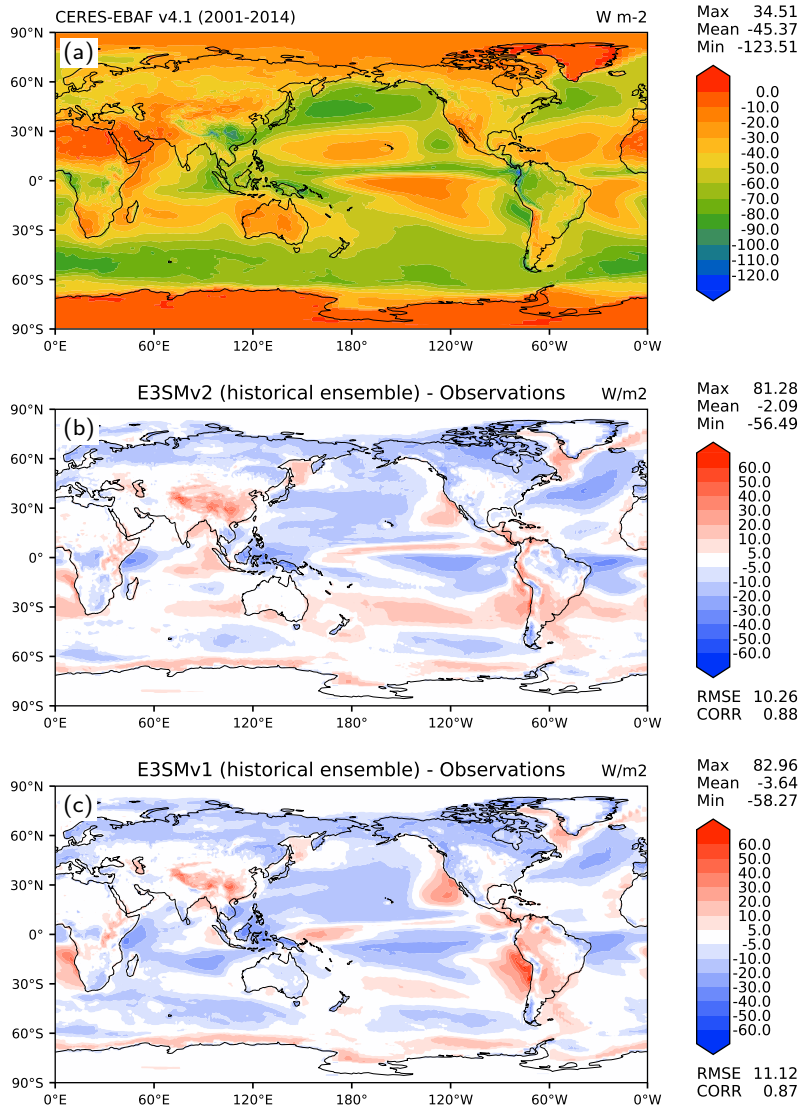

Figure S4. Annual top-of-atmosphere shortwave cloud radiative effect (SWCRE; W m^{-2}): (a) CERES-EBAF Ed4.1 observational estimate (2001-2014), (b) model bias from the 5-member ensemble of E3SMv2 historical coupled simulations (2001–2014), and (c) model bias from the 5-member ensemble of E3SMv1 historical coupled simulations (2001–2014). RMSE = root-mean-square error. CORR = correlation coefficient between observation and model.

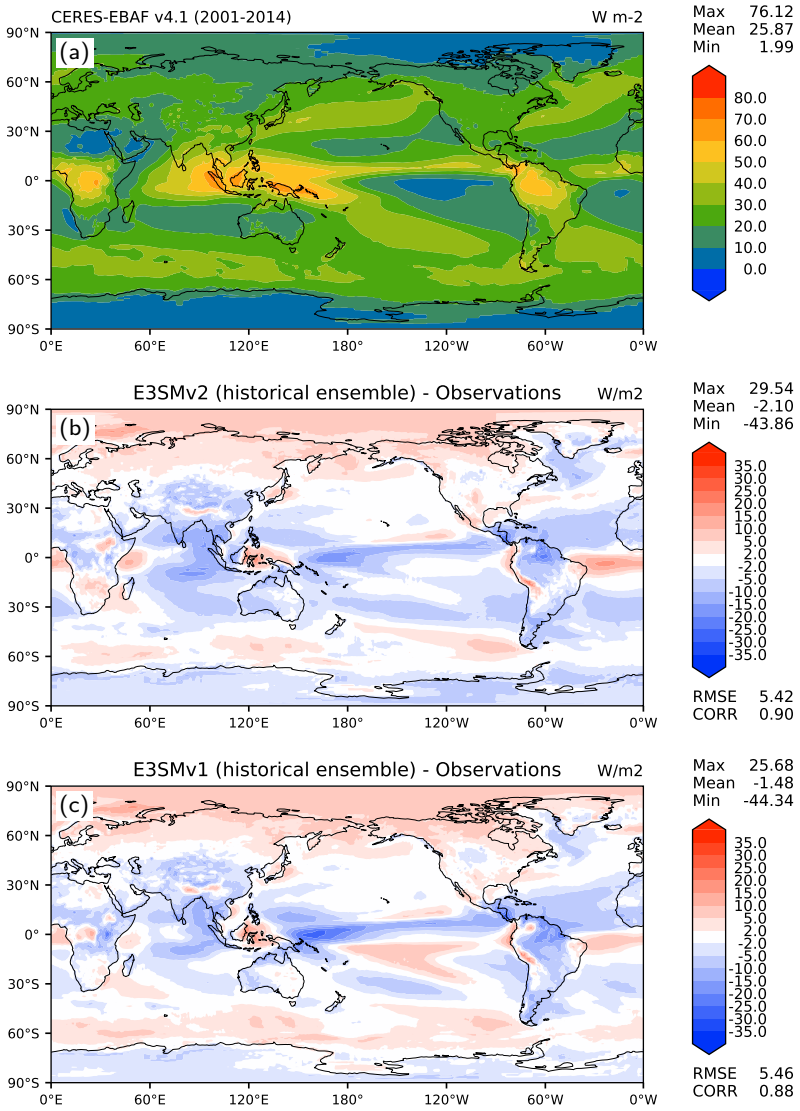

Figure S5. Annual top-of-atmosphere longwave cloud radiative effect (LWCRE; W m^{-2}): (a) CERES-EBAF Ed4.1 observational estimate (2001-2014), (b) model bias from the 5-member ensemble of E3SMv2 historical coupled simulations (2001–2014), and (c) model bias from the 5-member ensemble of E3SMv1 historical coupled simulations (2001–2014). RMSE = root-mean-square error. CORR = correlation coefficient between observation and model.

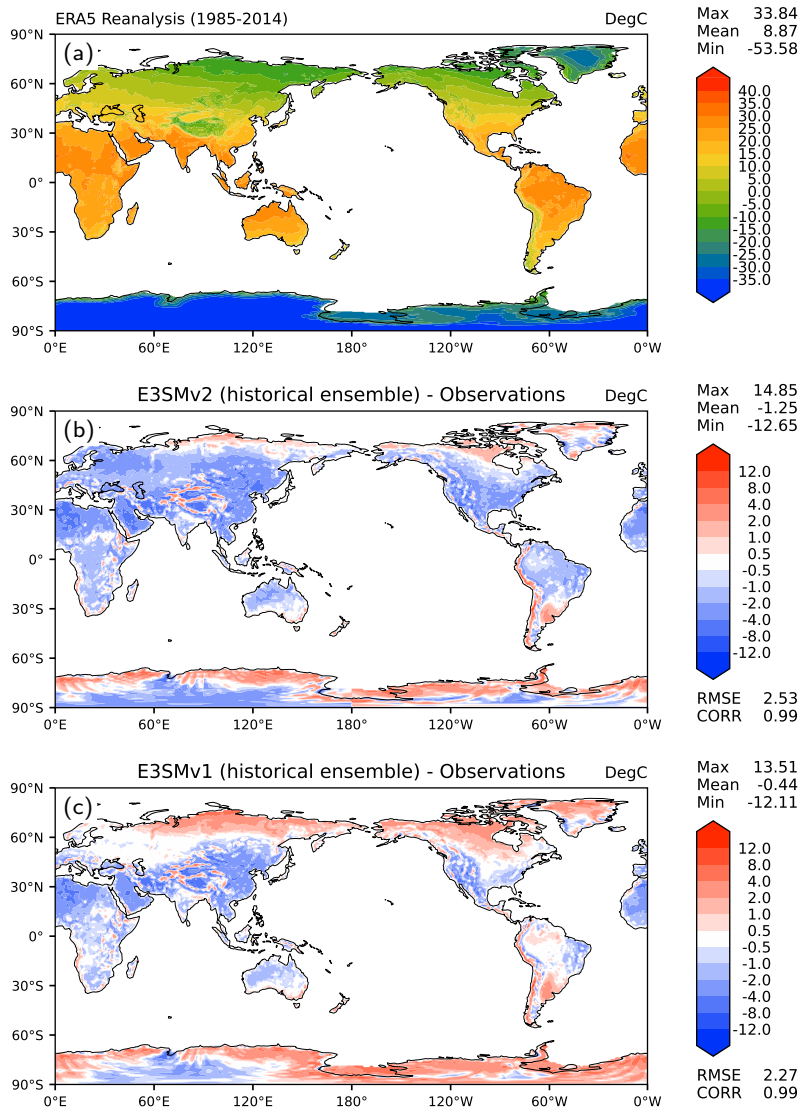

Figure S6. Annual surface air temperature over land (°C): (a) ERA5 reanalysis (1985-2014), (b) model bias from the 5-member ensemble of E3SMv2 historical coupled simulations (1985–2014), and (c) model bias from the 5-member ensemble of E3SMv1 historical coupled simulations (1985–2014). RMSE = root-mean-square error. CORR = correlation coefficient between observation and model.

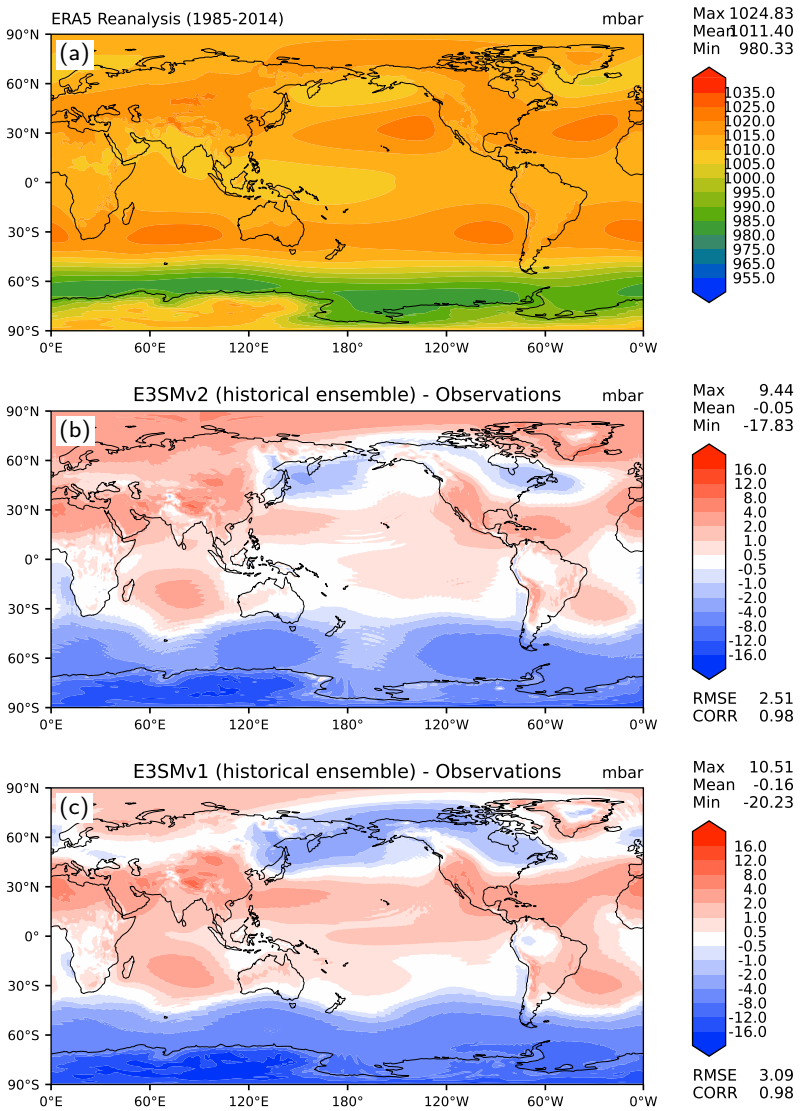

Figure S7. Annual mean sea-level pressure (hPa): (a) ERA5 reanalysis (1985-2014), (b) model bias from the 5-member ensemble of E3SMv2 historical coupled simulations (1985–2014), and (c) model bias from the 5-member ensemble of E3SMv1 historical coupled simulations (1985–2014). RMSE = root-mean-square error. CORR = correlation coefficient between observation and model.

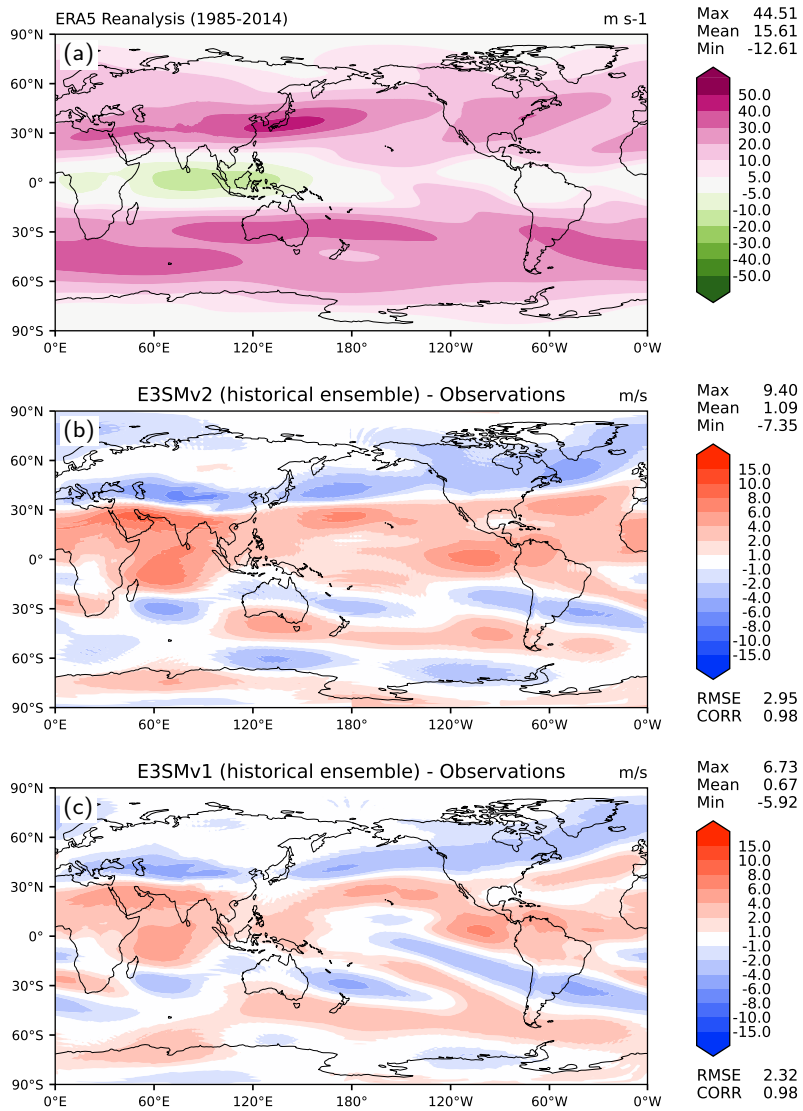

Figure S8. Annual mean 200-hPa zonal wind): (a) ERA5 reanalysis (1985-2014), (b) model bias from the 5-member ensemble of E3SMv2 historical coupled simulations (1985–2014), and (c) model bias from the 5-member ensemble of E3SMv1 historical coupled simulations (1985–2014). RMSE = root-mean-square error. CORR = correlation coefficient between observation and model.

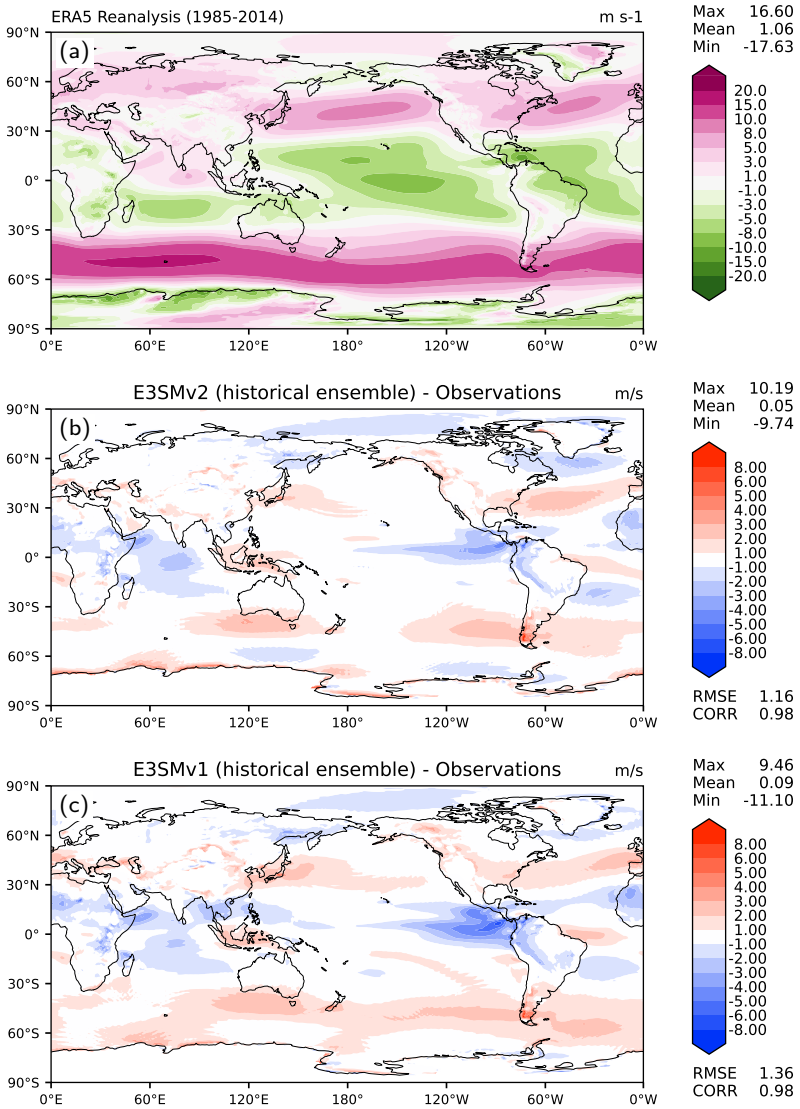

Figure S9. Annual mean 850-hPa zonal wind): (a) ERA5 reanalysis (1985-2014), (b) model bias from the 5-member ensemble of E3SMv2 historical coupled simulations (1985–2014), and (c) model bias from the 5-member ensemble of E3SMv1 historical coupled simulations (1985–2014). RMSE = root-mean-square error. CORR = correlation coefficient between observation and model.

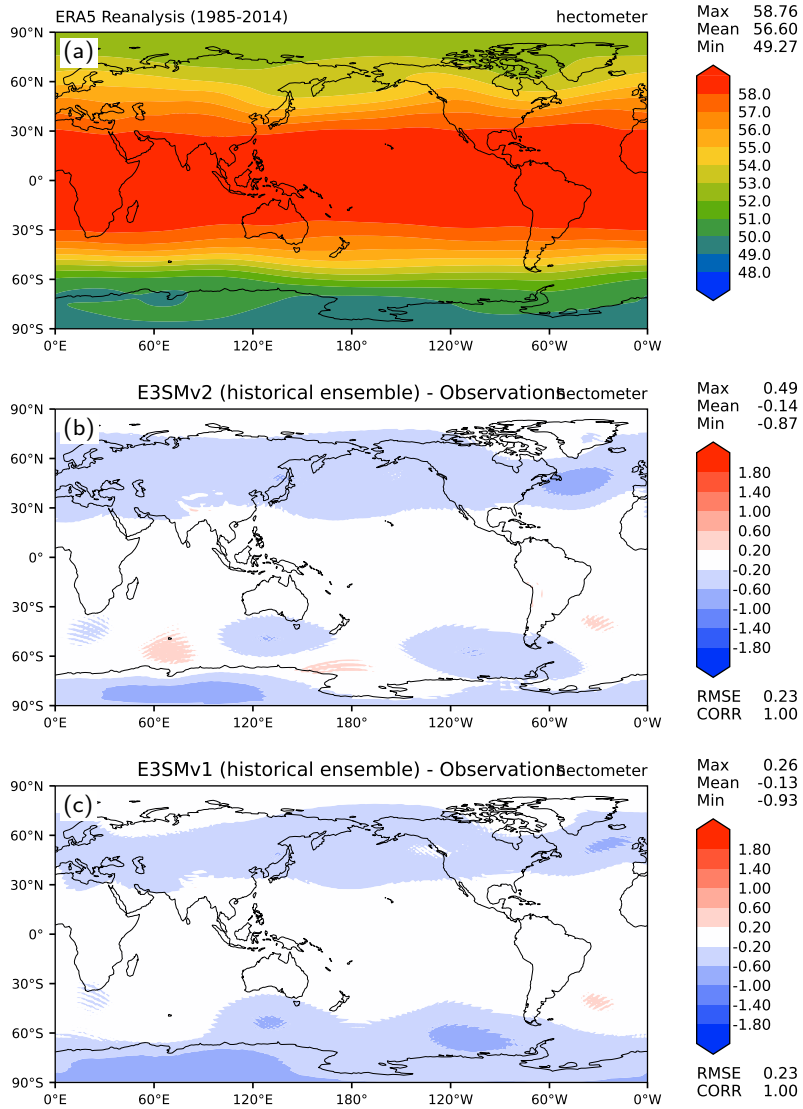

Figure S10. Annual mean 500-hPa geopotential height): (a) ERA5 reanalysis (1985-2014), (b) model bias from the 5-member ensemble of E3SMv2 historical coupled simulations (1985–2014), and (c) model bias from the 5-member ensemble of E3SMv1 historical coupled simulations (1985–2014). RMSE = root-mean-square error. CORR = correlation coefficient between observation and model.

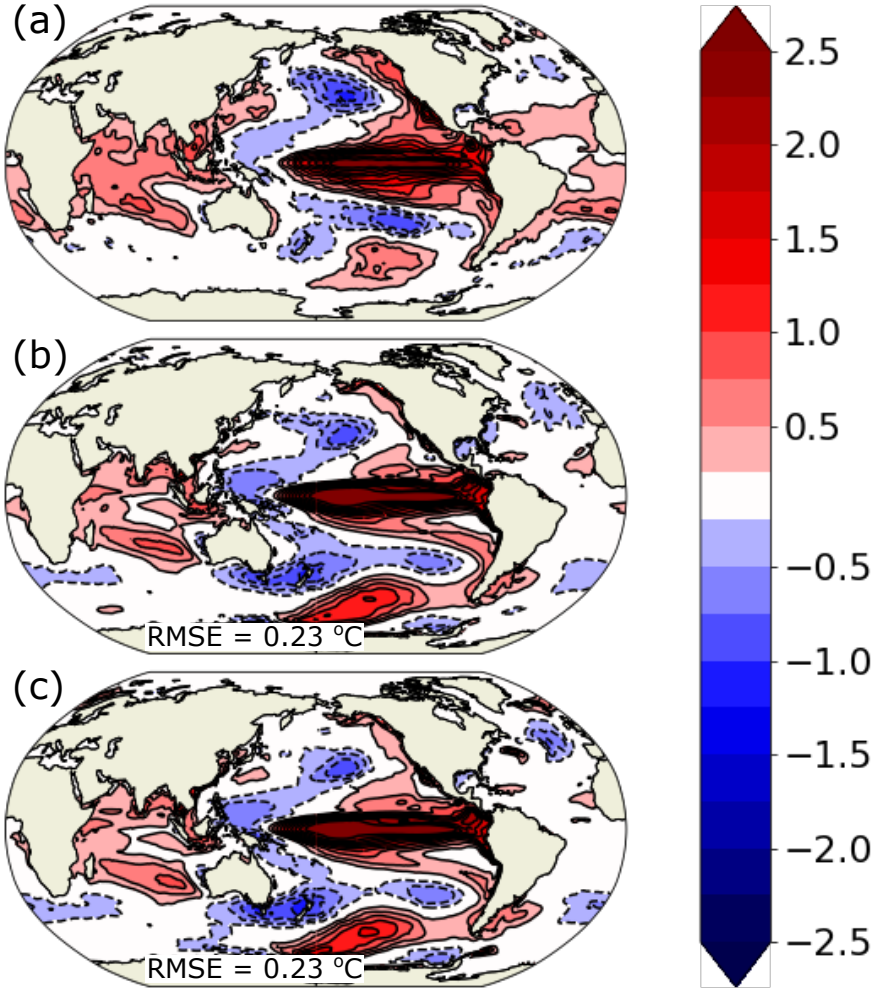

Figure S11. (a–c) Difference of composite El Niño events and composite La Niña events for the HadleyISST data set, the E3SMv2 historical ensemble (1850–2015), and the pre-industrial control, respectively. El Niño events are defined as periods when the Niño 3.4 SST anomaly exceeds 0.8 °C for more than six consecutive months. The La Niña criterion is Niño 3.4 SST anomaly less then -0.8 °C for more than 6 months (these definitions are consistent with Menary et al., 2018). When an El Niño–Southern Oscillation event is identified, the SST is averaged from November to March. For model output, every ensemble member contributes to the mean composite.

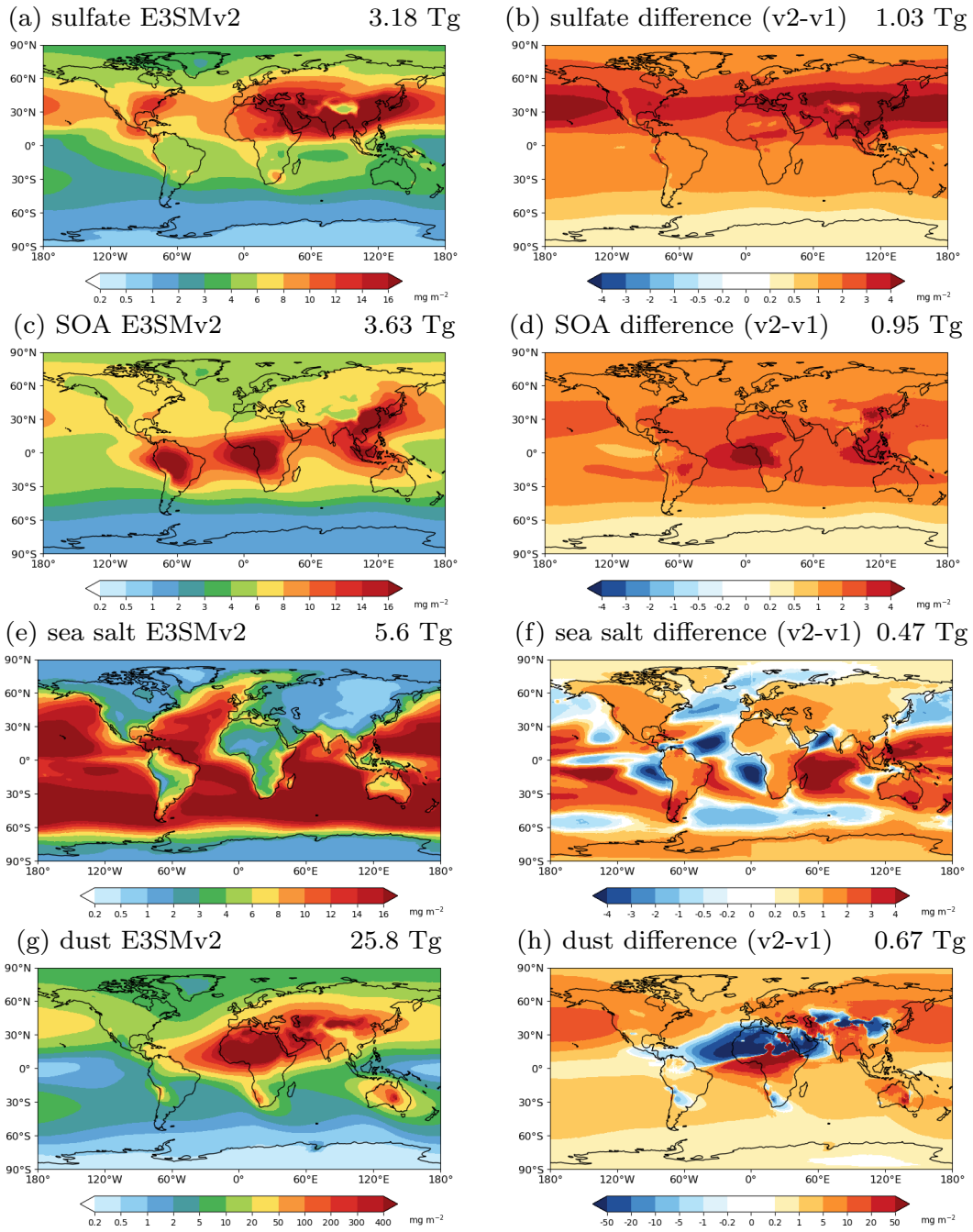

Figure S12. Spatial distributions of global annual mean (2000-2014) aerosol burdens from E3SMv2 historical simulations: (a) sulfate, (c) SOA, (e) sea salt, and (g) dust. Also shown are the burden differences between E3SMv2 and E3SMv1 historical simulations: (b) sulfate, (d) SOA, (f) sea salt, and (h) dust.

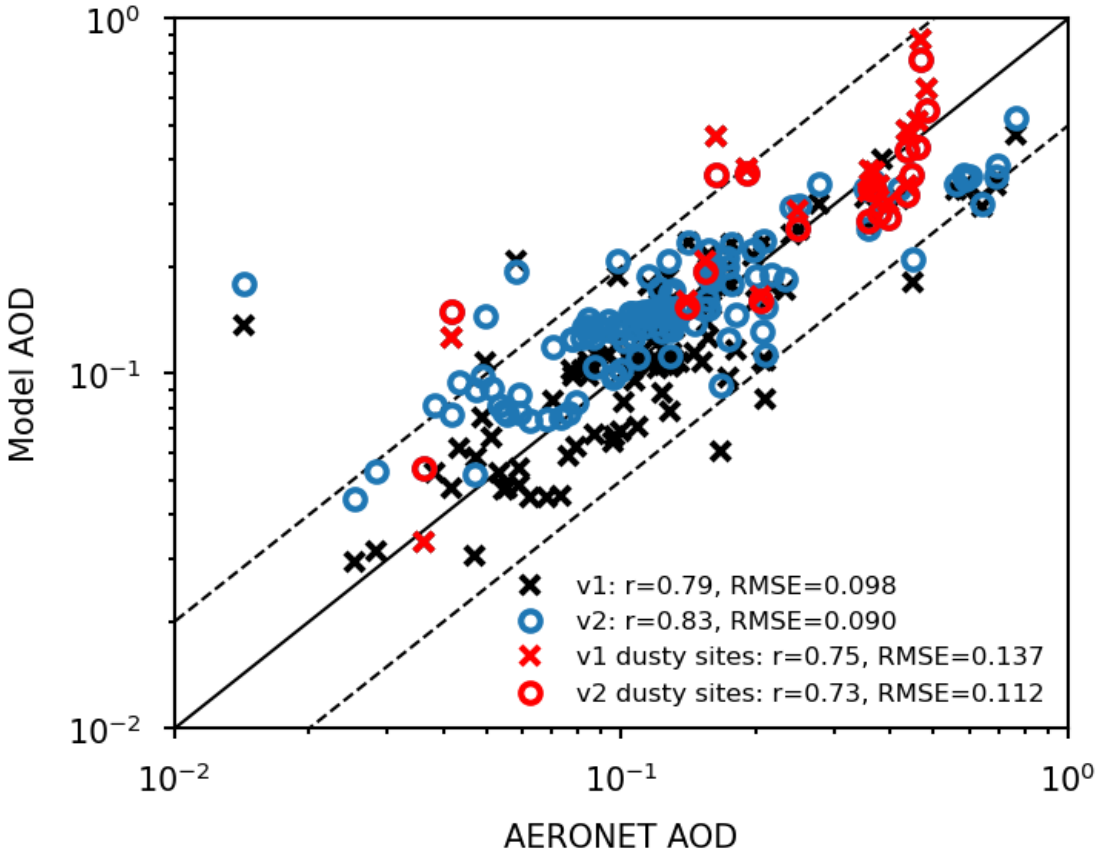

Figure S13. Comparison of the E3SMv2 aerosol optical depth (AOD) at $550nm$ with the AERONET measurements between 2006-2015.

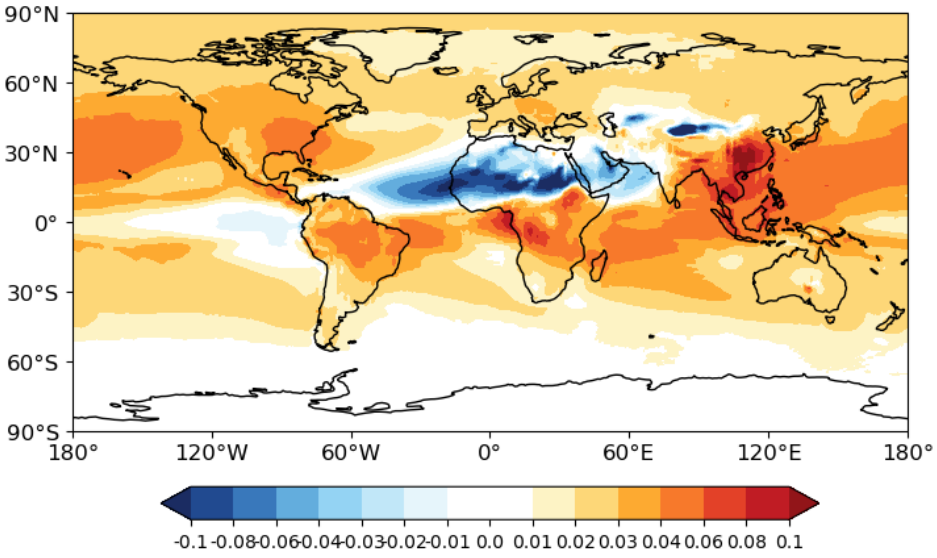

(a) AOD differences

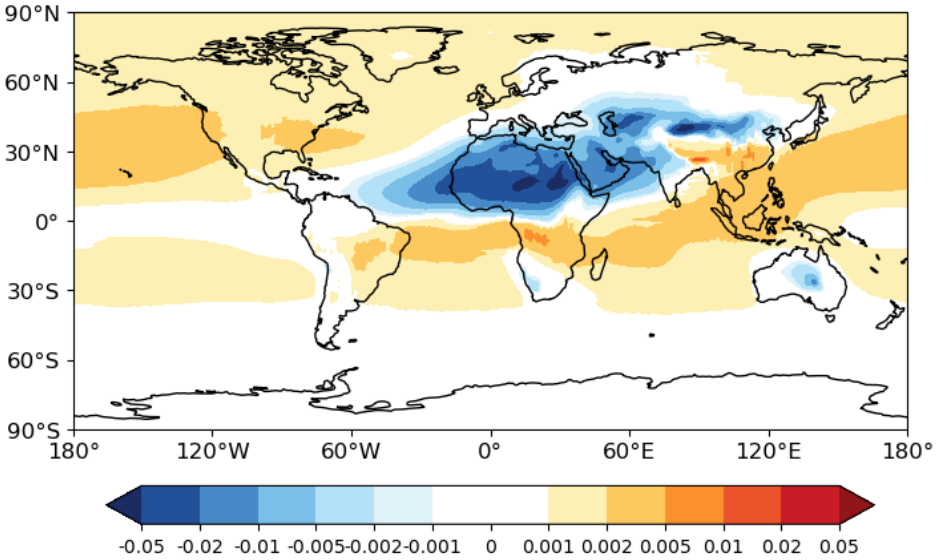

(b) AAOD differences

Figure S14. Differences in (a) AOD and (b) AAOD between E3SMv2 and E3SMv1 in 2000-2014.

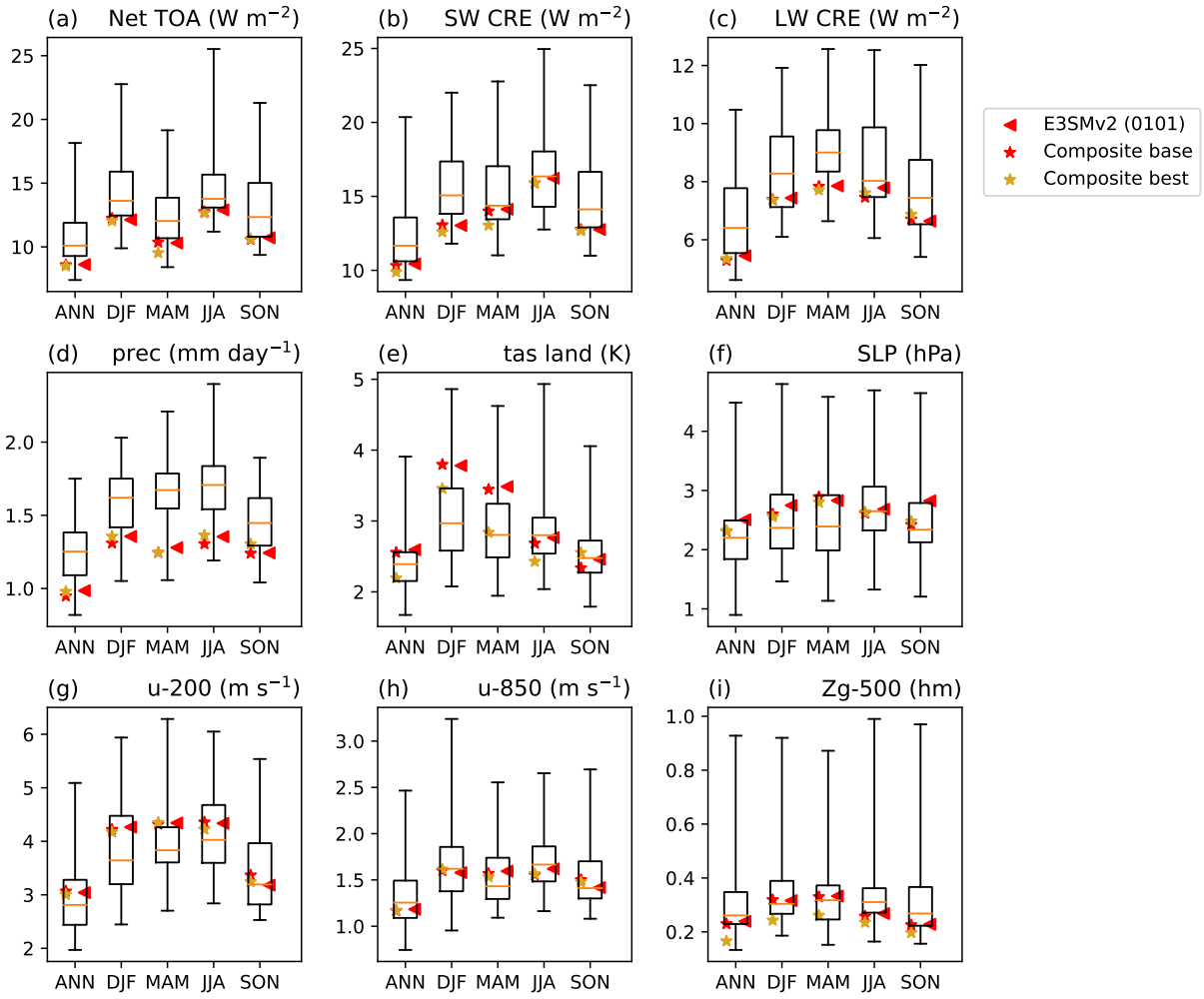

Figure S15. Same as Figure 7 but showing first historical member of E3SMv2 (red triangles) and composite configurations. Red stars (composite base) and gold stars (composite best) refer to hypothetical composite configurations generated by linear combination of single-forcing simulations described in Section 5. Complete data is available in Table S1.

Table S1. Data from Figures 7 and S15 is available in external file '`cmip6.csv`'. Rows correspond to CMIP6 models (first member of historical simulations) or E3SMv2 configurations and column correspond to different fields and seasons. Values are RMSE against relevant observations. Missing values (models for which a specific variable is not available) are indicated by '`--`'. Underlying E3SM Diags comparison figures are available on-line (`https://portal.nersc.gov/project/e3sm/CMIP6_E3SMv2_Golaz_et_al_2022`) . See main text for additional information.